

Electronic Supplementary Information

A dual-responsive nanozyme sensor with ultra-high sensitivity and ultra-low cross-interference towards metabolic biomarkers monitoring

Xinyu Wang,^a Zhaoping Xia,^a Essy Kouadio Fodjo,^b Wei Deng^{* a} and Dan Li^{* a}

^a School of Chemical and Environmental Engineering, Shanghai Institute of Technology, Shanghai 201418, P. R. China.

^b Laboratory of Physical Chemistry, UFR SSMT, Felix Houphouet Boigny University, 22 BP 582 Abidjan 22, Cote d'Ivoire

* Corresponding author phone/fax: +86-21-60873241; E-mail: dany@sit.edu.cn (D. Li)

S1. Experimental sections

S1.1 Synthesis of PEG-SH-modified GNPs

GNPs of different sizes were prepared in aqueous solution by controlling the ratios of concentrations of sodium citrate and HAuCl₄.¹ Briefly, hydrogen tetrachloroaurate (III) trihydrate (HAuCl₄·3H₂O) (2.0 mL, 0.1 mM) in deionized water and 0.5 mL of 0.05 M sodium citrate in deionized water were first mixed with 100 mL of deionized H₂O in a 200 mL flask. The stirring of the reaction mixture was kept at room temperature for 30 min. Then, 0.15 mL of 0.1 M freshly prepared sodium borohydride (NaBH₄) was added to the mixture under stirring and the color of solution changed from colorless to orange. Afterward, the stirring was stopped and the resultant solution was left undisturbed for 1 h. The synthesized GNPs were ~50 nm in diameter.

PEG-SH-modified GNPs was obtained by a ligand exchange procedure. Specifically, 10 mL of GNPs solution was centrifuged at 8,000 rpm for 10 min to remove citrate in the solution. The precipitate was then re-dispersed in water (10 mL), and subsequently 0.5 mL of 10 mM PEG-SH was added dropwise under vigorous stirring. Excess PEG-SH was removed by centrifugation at 8,000 rpm for 10 min. the concentration of PEG-SH-modified GNPs was estimated according to the concentration of GNPs by the method reported previously.²

S1.2 Raman enhancement factor calculation

The enhancement factor (*EF*) can be calculated using the following formula:

$$EF = (I_{SERS} / I_{bulk}) \times (N_{bulk} / N_{SERS})$$

where I_{SERS} and I_{bulk} are the vibration intensities in the SERS of caffeine and normal Raman spectra of caffeine, respectively. N_{bulk} and N_{SERS} are the number of molecules under laser illumination for the bulk sample, and the number of molecules in the self-assembled monolayers (SAMs), respectively. The N_{SERS} and N_{bulk} values can be calculated on the basis of the estimate of the concentration of surface species or bulk sample and the corresponding sampling areas. It is reported that the average surface density of caffeine molecules in densely packed monolayers is approximately one caffeine molecule per 0.5 nm².³ Then the surface coverage of caffeine monolayer on GNPs@NH₂-MIL53 is 3.32×10^{-10} mol cm⁻² ($\Gamma = 1 / [(0.5 \times 10^{-14}) \times (6.02 \times 10^{23})]$ mol cm⁻² = 3.32×10^{-10} mol cm⁻²). Taking the sampling area (*ca.* 10 μm in diameter) into account, N_{SERS} has a value of 2.61×10^{-16} mol ($N_{SERS} = \Gamma \times \pi \times (10/2)^2 \mu\text{m}^2 = 2.61 \times 10^{-16}$ mol). For the solid sample, the sampling volume is the product of the area of the laser spot (*ca.* 10 μm diameter) and the penetration depth (~40 μm) of the focused laser beam. Assuming the density of bulk caffeine is 1.23 g cm⁻³ (<https://www.sigmaaldrich.cn/CN/zh/product/sial/c6035?context=product>), N_{bulk} can be calculated to be 1.99×10^{-11} mol ($N_{bulk} = 1.23 \text{ g cm}^{-3} \times \pi \times 25 \mu\text{m}^2 \times 40 \mu\text{m} / (194.19 \text{ g mol}^{-1}) = 1.99 \times 10^{-11}$ mol). For the vibrational mode at 1283 cm⁻¹, the ratio of I_{SERS} to I_{bulk} was about 35.2 (Fig S4), so *EF* was

calculated to be 2.68×10^6 ($35.2 \times [1.99 \times 10^{-11} / (2.61 \times 10^{-16})] = 2.68 \times 10^6$).

S1.3 Calculation methods

HOMO-LUMO calculations have been carried out by the latest version of ORCA quantum chemistry software (Version 5.0.1). The corrected version of B97 exchange-correlation functional proposed by Grimme (so-called B97-3c) was adopted for all calculations at default temperature conditions (298.15K). The B97-3c functional which is based on the well-known B97 functional, is a highly efficient method which utilizes three corrections namely: the D3BJ method including three-body term to account for long-range dispersion interactions, a short range bond-length correction (SRB) which corrects for systematically overestimated covalent bond-lengths for electronegative elements and a modified stripped-down triple- ζ basis (def2-mTZVP) to obtain accurate geometries and relative energies. The nature of noncovalent interaction was studied by using IGM method through Multiwfn software.⁴ The visualization of IGM and orbitals were rendered by VMD. The binding energy between caffeine and APA was calculated by the following formula:⁵

$$E_{\text{binding}} = E_{\text{complex}} - (E_{\text{caffeine}} + E_{\text{APA}})$$

S2. Additional Figures and Tables

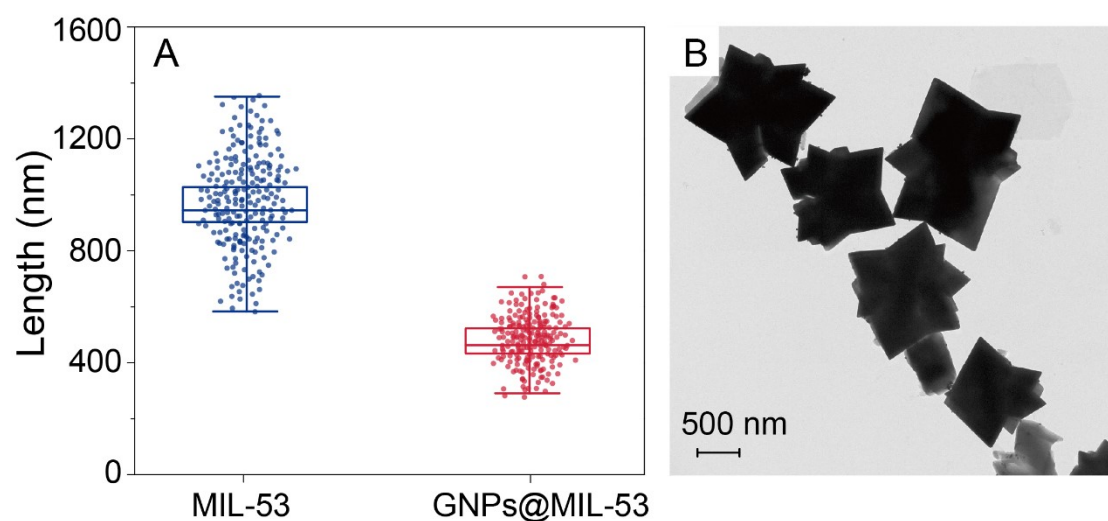


Fig. S1 (A) Size-distribution of GNPs@MIL-53 and MIL-53 nanoparticles. (B) Representative TEM micrographs of MIL-53 crystallites. Length measured along the principal prolate axis.

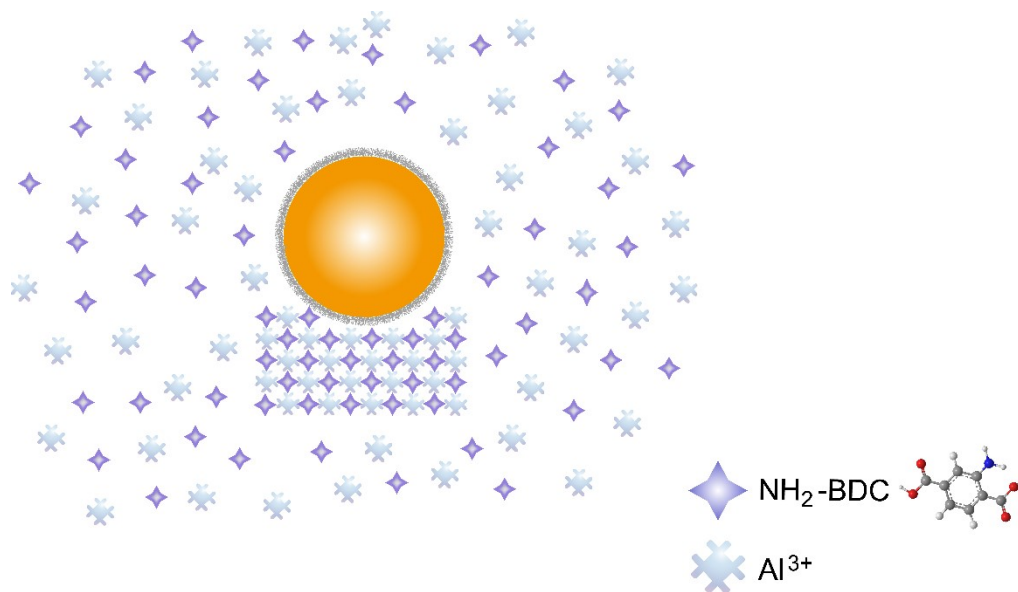


Fig. S2 Interactions between PEG-SH and 2-aminoterephthalic acid (NH₂-BDC) make nucleation more favorable on the GNPs.

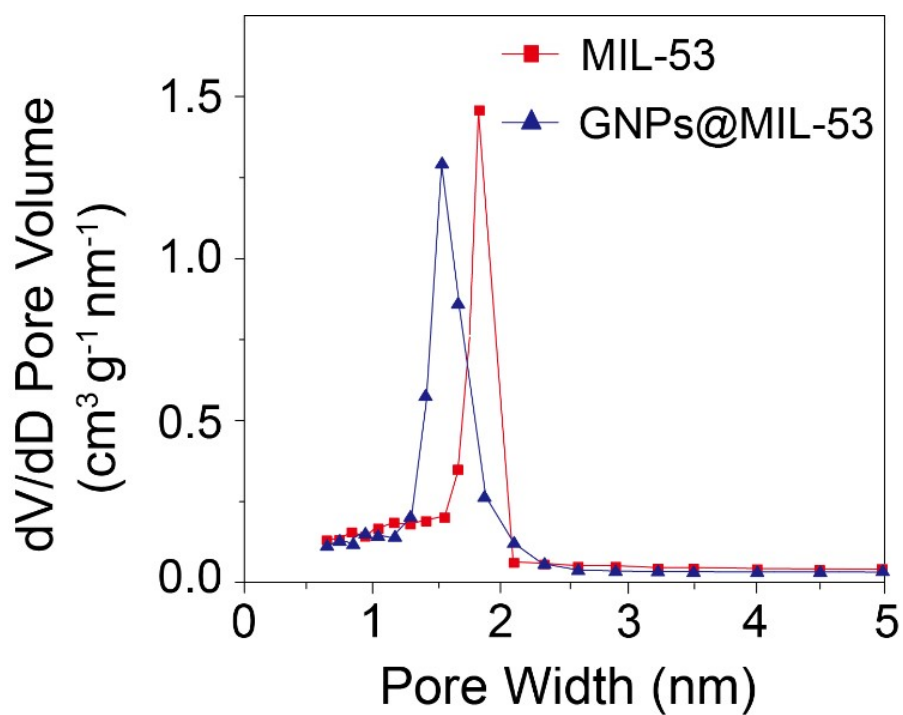


Fig. S3 The differential pore size distributions of MIL-53 and GNPs@MIL-53.

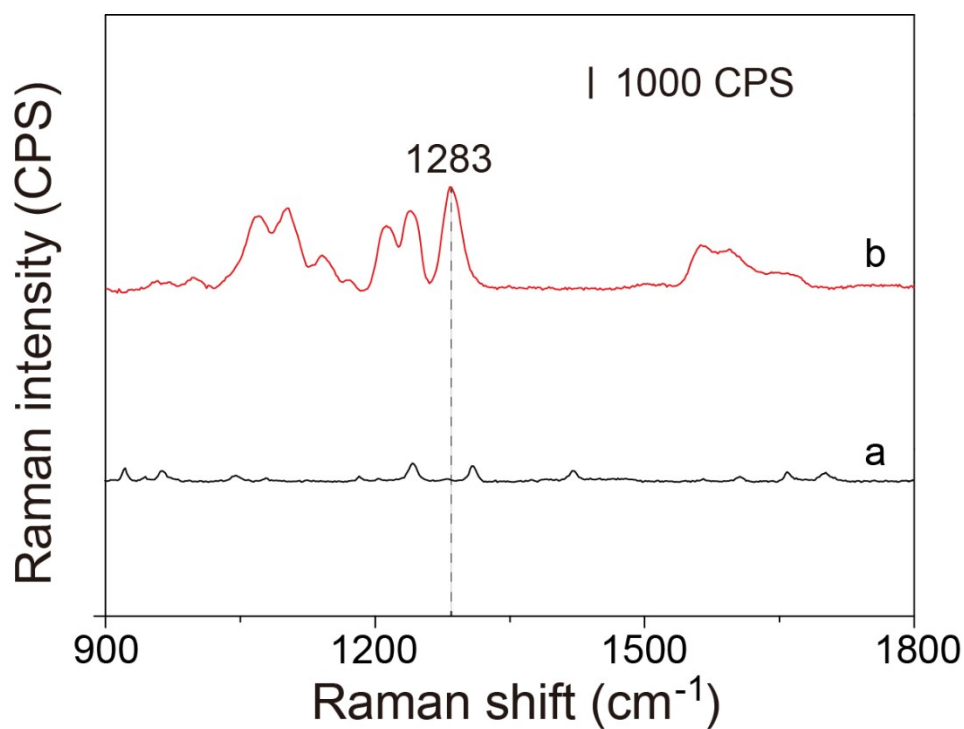


Fig. S4 (a) Normal Raman spectrum of solid caffeine; (b) SERS spectra of GNPs@MIL-53 DPC after adsorption of caffeine with the concentration of 1 μM , respectively.

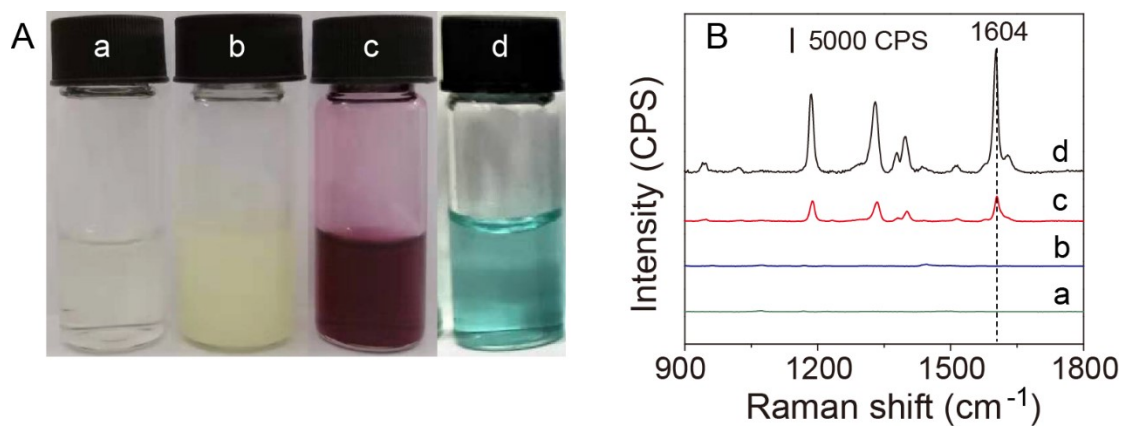


Fig. S5 (A) Photo and (B) corresponding SERS spectra of the samples containing (a) TMB + H_2O_2 (control), (b) TMB + H_2O_2 + MIL-53, (c) TMB + H_2O_2 + AuNPs, and (d) TMB + H_2O_2 + GNPs@MIL-53 in 10 mM PBS (pH=6.0).

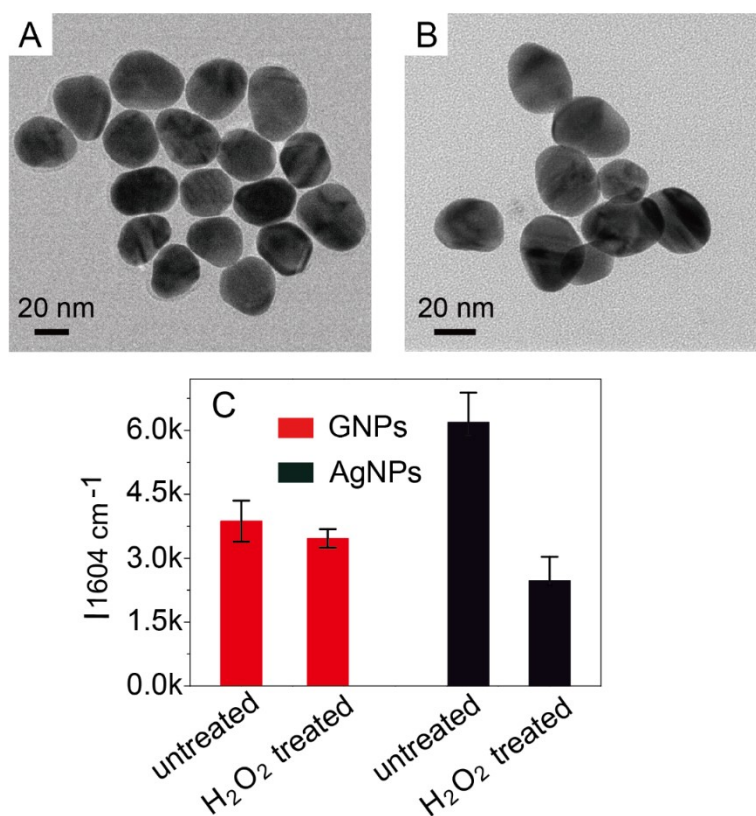


Fig. S6 TEM image of (A) citrate-protected GNPs and (B) citrate-modified AgNPs. (C) SERS performances of GNPs and AgNPs without or with 1 mM H_2O_2 treatment. Error bars indicate standard deviations of three independent measurements.

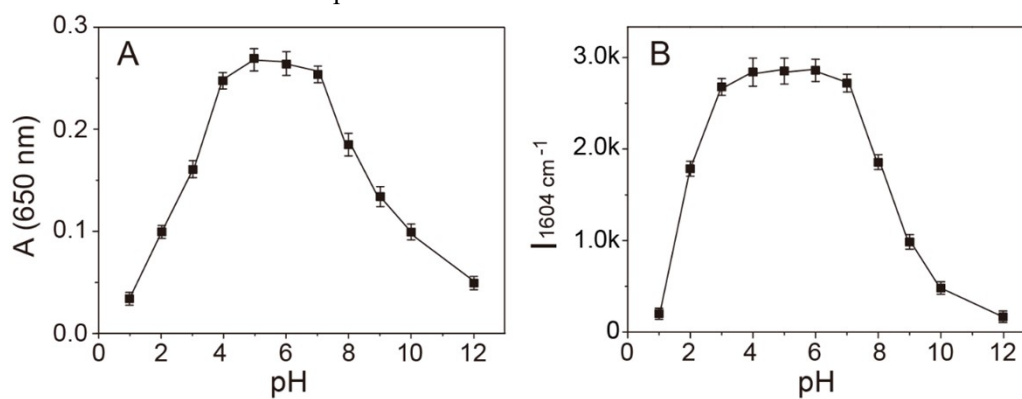


Fig. S7 The effects of temperature on the (A) absorbance at 650nm ($A_{650 \text{ nm}}$) and (B) Raman intensity at 1604 cm^{-1} ($I_{1604 \text{ cm}^{-1}}$) of GNPs@MIL-53 with the presence of glucose at 50 μM and 10 μM , respectively. Each data point represents the average value from three measurements on the same samples. Error bars show the standard deviations.

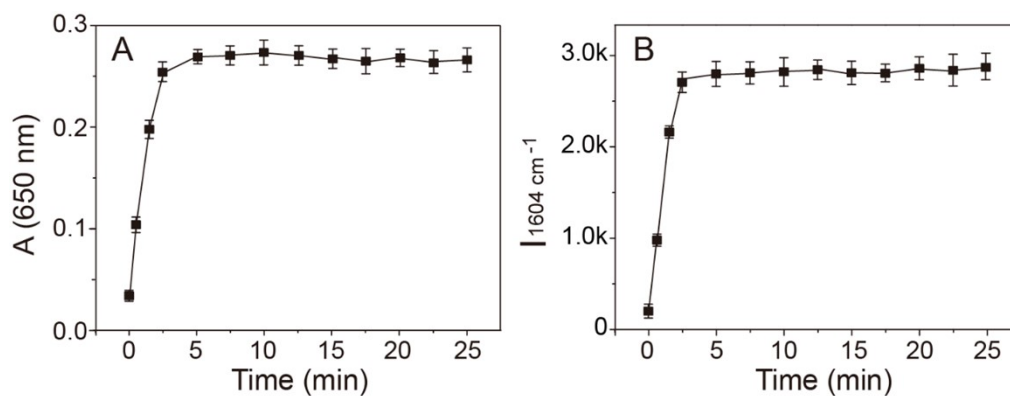


Fig. S8 The effects of incubation time on the (A) absorbance at 650nm ($A_{650 \text{ nm}}$) and (B) Raman intensity at 1604 cm^{-1} ($I_{1604 \text{ cm}^{-1}}$) of GNPs@MIL-53 with the presence of glucose at 50 μM and 10 μM , respectively. Each data point represents the average value from three measurements on the same samples. Error bars show the standard deviations.

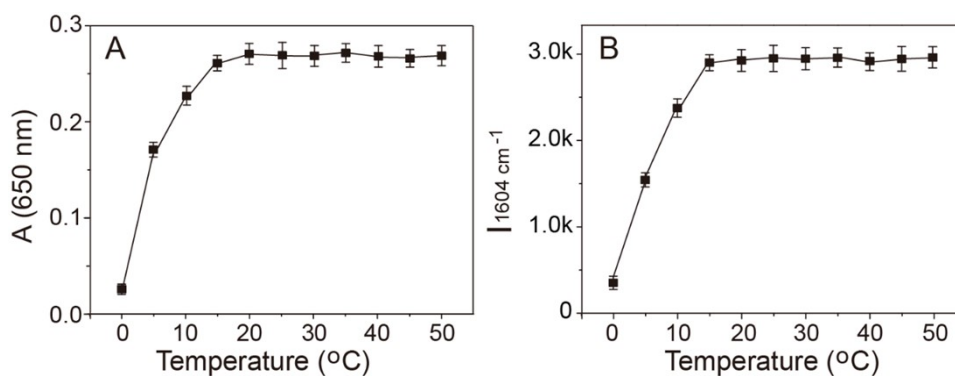


Fig. S9 The effects of temperature on the (A) absorbance at 650nm ($A_{650 \text{ nm}}$) and (B) Raman intensity at 1604 cm^{-1} ($I_{1604 \text{ cm}^{-1}}$) of GNPs@MIL-53 with the presence of glucose at 50 μM and 10 μM , respectively. Each data point represents the average value from three measurements on the same samples. Error bars show the standard deviations.

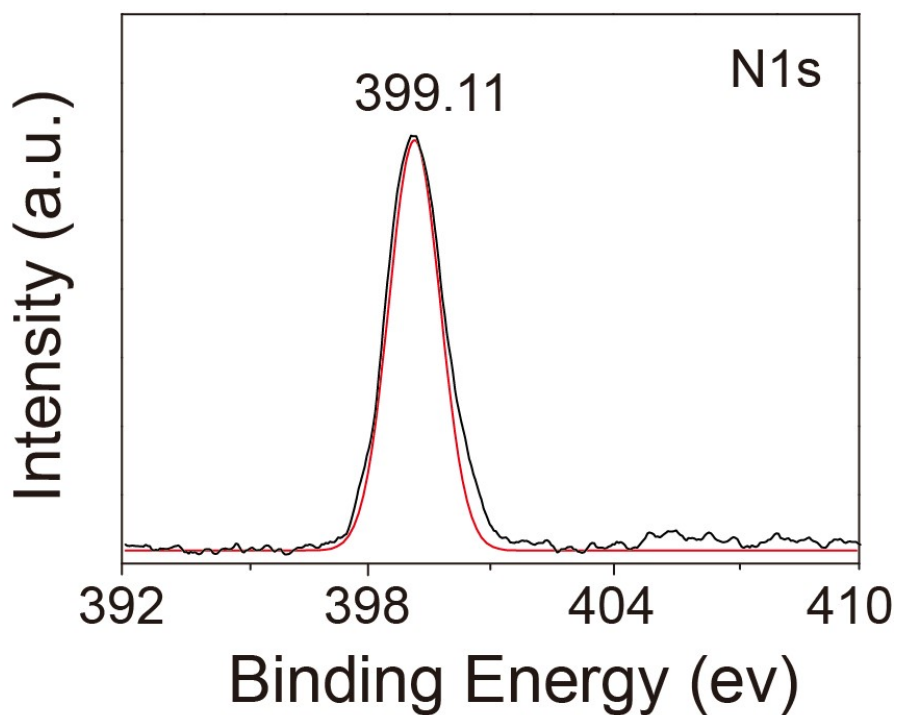


Fig. S10 XPS results of N 1s region for GNPs@MIL-53.

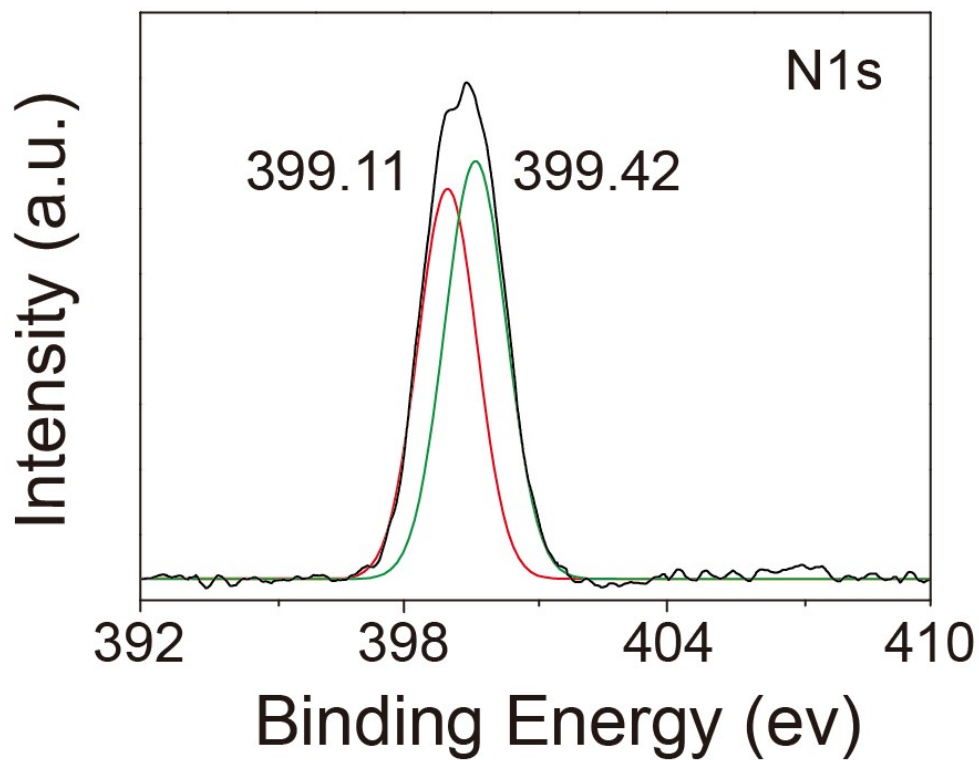


Fig. S11 XPS results of N 1s region for GNPs@MIL-53 after adding caffeine.

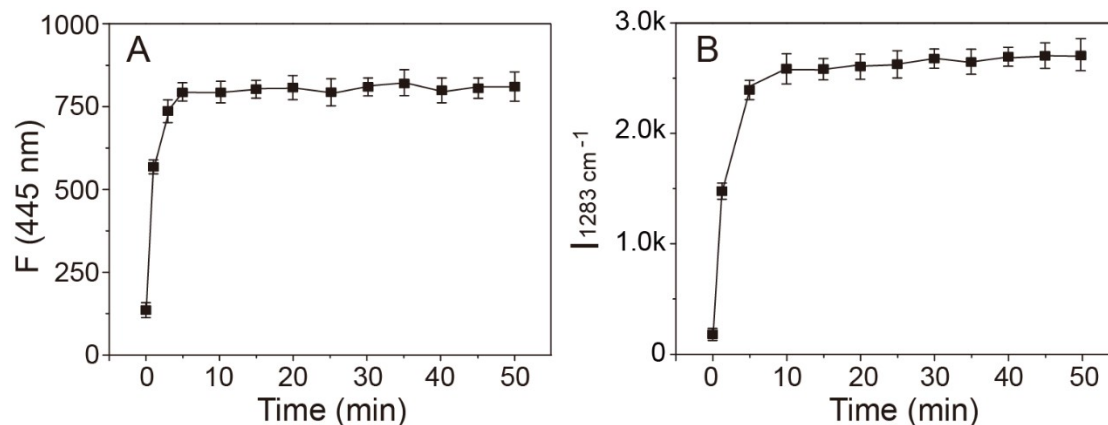


Fig. S12 The effects of incubation time on the (A) FL intensity at 445 nm ($F_{445 \text{ nm}}$) and (B) Raman intensity at 1283 cm^{-1} ($I_{1283 \text{ cm}^{-1}}$) of GNPs@MIL-53 with the presence of caffeine at 100 μM and 10 μM , respectively. Each data point represents the average value from three measurements on the same samples. Error bars show the standard deviations.

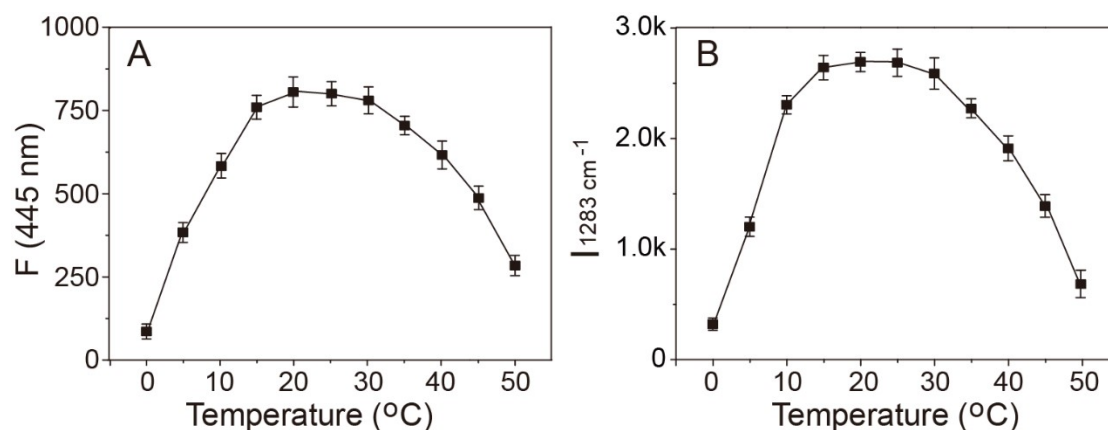


Fig. S13 The effects of temperature on the (A) FL intensity at 445 nm ($F_{445 \text{ nm}}$) and (B) Raman intensity at 1283 cm^{-1} ($I_{1283 \text{ cm}^{-1}}$) of GNPs@MIL-53 with the presence of caffeine at 100 μM and 10 μM , respectively. Each data point represents the average value from three measurements on the same samples. Error bars show the standard deviations.

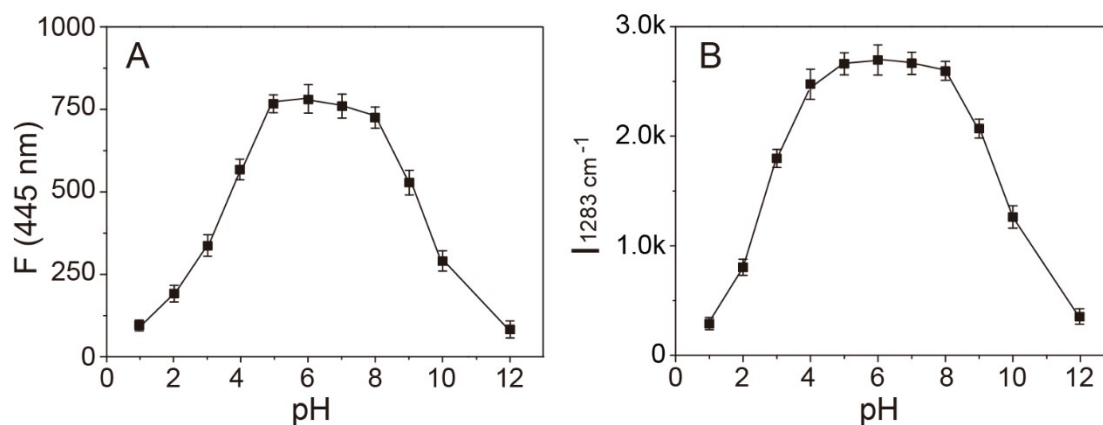


Fig. S14 The effects of temperature on the (A) FL intensity at 445 nm ($F_{445 \text{ nm}}$) and (B) Raman intensity at 1283 cm^{-1} ($I_{1283 \text{ cm}^{-1}}$) of GNP@MIL-53 with the presence of caffeine at 100 μM and 10 μM , respectively. Each data point represents the average value from three measurements on the same samples. Error bars show the standard deviations.

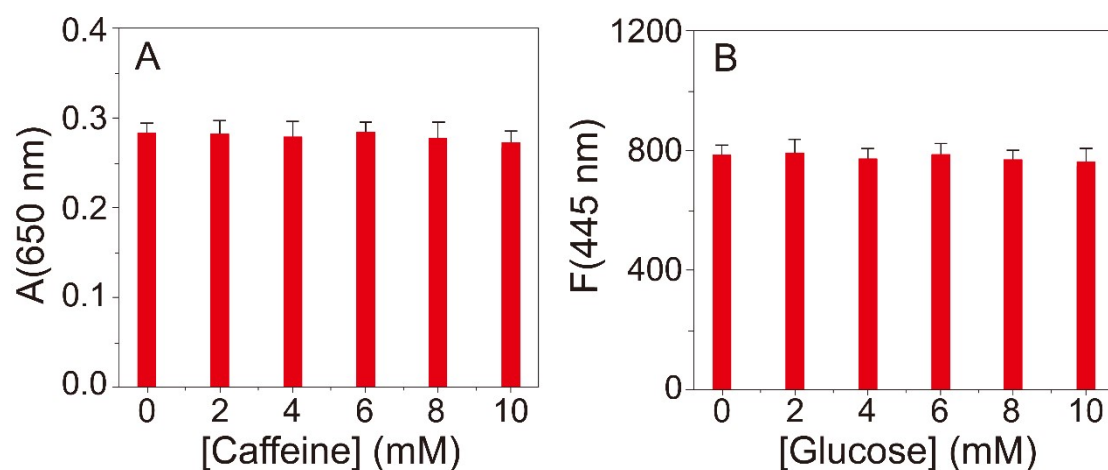


Fig. S15 (A) The absorbance at 650 nm ($A_{650 \text{ nm}}$) of 50 μM glucose under different caffeine concentrations. (B) The FL intensity at 445 nm ($F_{445 \text{ nm}}$) of 50 μM caffeine under different glucose concentrations.

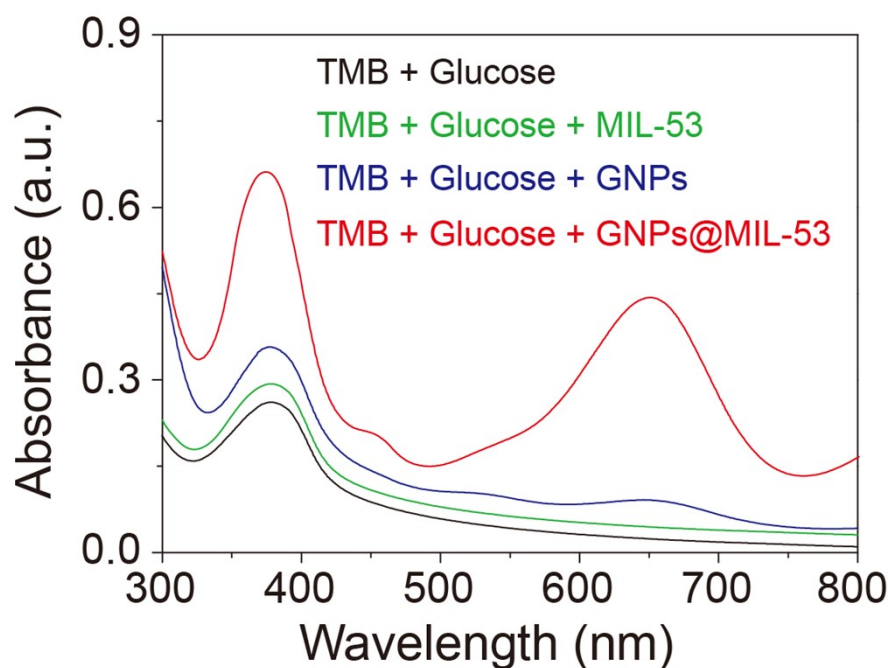


Fig. S16. The absorption spectra of various TMB based systems.

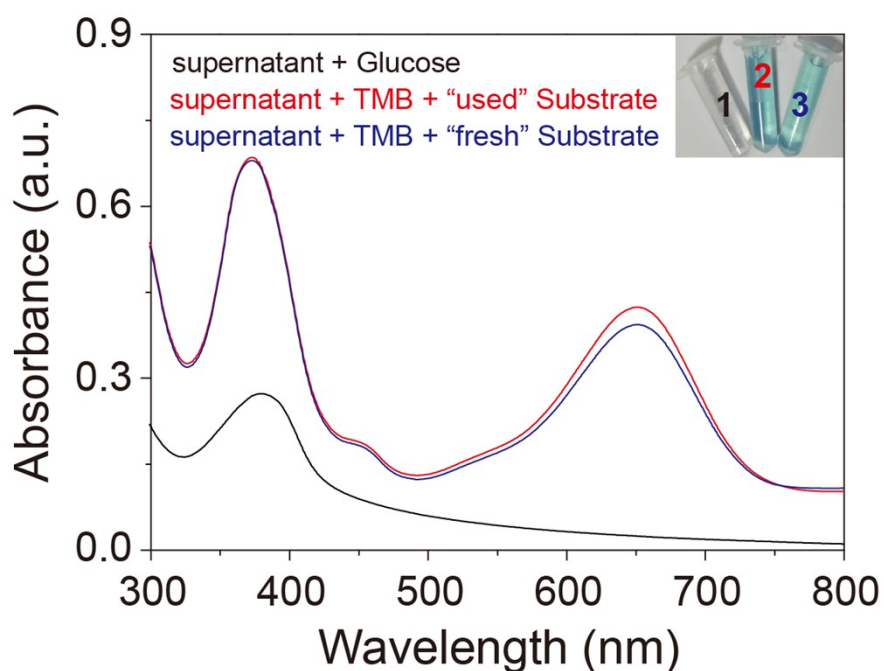


Fig. S17 Absorption spectra of TMB chromogenic reaction systems. The supernatant came from the GNPs@MIL-53-glucose system. After catalysis, the GNPs@MIL-53 were separated by centrifugation, and the resulting supernatant was obtained. The “used” substrate meant the GNPs@MIL-53 had been used for the first-step GOx-like catalysis. The “fresh” substrate meant the GNPs@MIL-53 had not been employed for the catalysis of glucose oxidation.

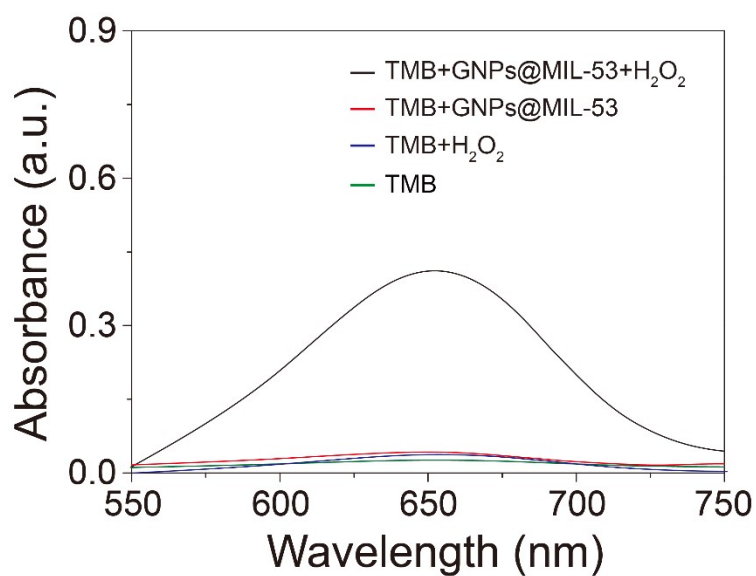


Fig. S18 UV-vis absorption of TMB corresponding to GNPs@MIL-53 and control in the deoxidized solution.

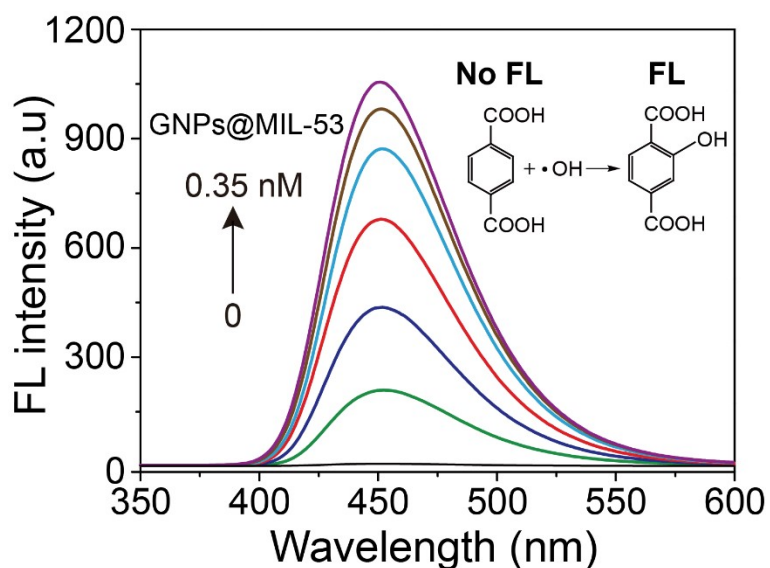


Fig. S19 The effects of GNPs@MIL-53 on the formation of $\cdot\text{OH}$ with terephthalic acid as a fluorescence probe. 5 mM of H_2O_2 , 0.2 mM of terephthalic acid and different concentrations of the GNPs@MIL-53 were incubated in PBS solutions (0.1 M, pH 6.0) and then exposed to 365-nm excitation for 10 min before fluorescence measurements.

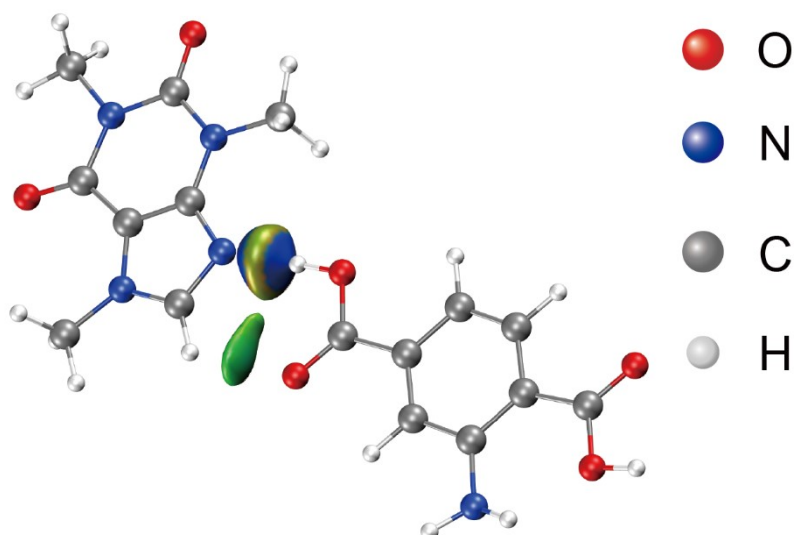


Fig. S20 IGM plots of caffeine-APA cocrystal. The blue and green scale colors on the surfaces denote strong and weak attractive interactions, respectively.

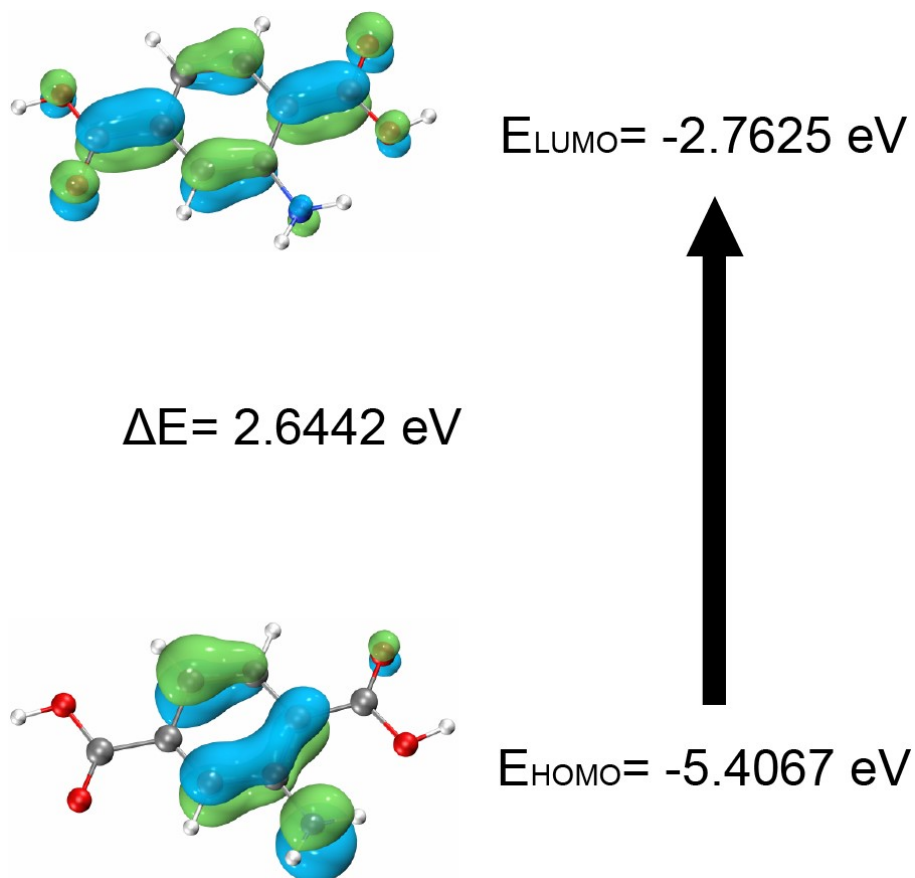


Fig. S21 The HOMO-LUMO energy gap of APA ligand.

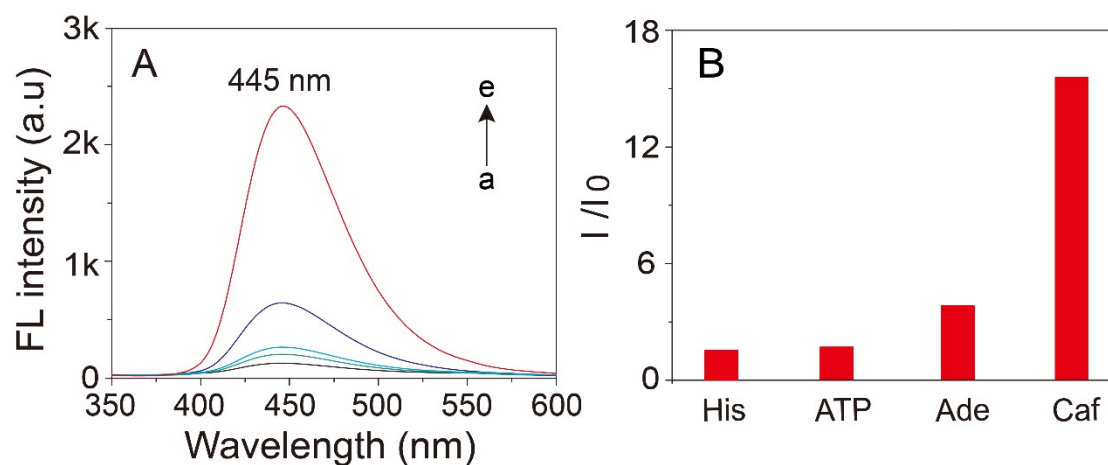


Fig. S22 (A) FL spectra of GNPs@MIL-53 (a) without and with the presence of (b) histidine (His), (c) adenosine triphosphate (ATP), (d) adenine (Ade), and (e) caffeine (Caf) at 10 μM . (B) The obtained FL enhancement (I/I_0) in part (A).

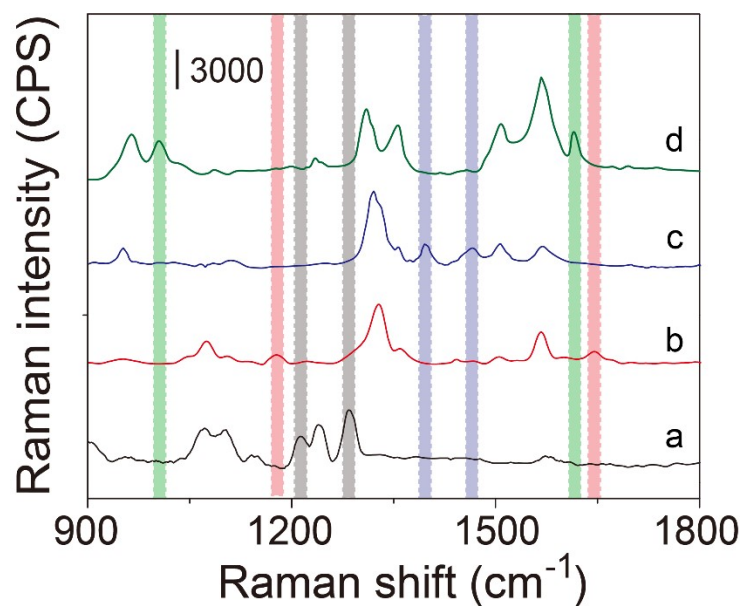


Fig. S23 SERS response of GNPs@MIL-53 toward (a) caffeine (Caf), (b) adenosine triphosphate (ATP), (c) adenine (Ade), and (d) histidine (His). The green, red, black and blue zones indicate the representative vibration peaks of the targeted analytes.

Table S1 Comparing the detection performance of different methods for glucose sensing.

Methods	Materials	Linearity (μM)	LOD (μM)	References
Colorimetric	Photonic IPN _{APBA}	1000-12000	350	[6]
Colorimetric	Resorcinol formaldehyde resins	200-8500	9.2	[7]
Colorimetric	Papain	50-500	25	[8]
SERS	AgNP/PATP-PMBA	30-20000	10	[9]
SERS	AuNPs@MIL-101@GOx	10-200	4.2	[10]
SERS	AgNRs@Al ₂ O ₃	1-3000	0.1	[11]
Fluorescence	C-dots/AgNPs	2-4000	1.39	[12]
Fluorescence	carbon nanoparticles	500-2000	10	[13]
Electrochemistry	Zn-CuO	25-500	1.5	[14]
Electrochemistry	Ni-Mn-S/TM	120-3500	4.8	[15]
Colorimetric/SERS	GOx-GNPs@NH ₂ -MIL 53(Al)	1-1000 / 0.1-5000	0.5 / 0.03	This work

Table S2 Comparing the detection performance of different methods for caffeine sensing.

Methods	Materials	Linearity (μM)	LOD (μM)	References
Electrochemistry	Graphene	2.6-210	0.28	[16]
Electrochemistry	Fe-doped MgNi ₂ O ₃	50-4000	0.276	[17]
Electrochemistry	HA-GN-MWCNT	2.35-169.35	0.938	[18]
Fluorescence	Sulfur-doped carbon quantum dots	0.2-70	0.05	[19]
Fluorescence	Glibenclamide	5.15-515	0.515	[20]
Fluorescence	3,5-diaminobenzoic acid	0.1-100	0.03	[21]
SERS	AgNPs@MISPE	5.15×10^{-4} - 5.15×10^{-2}	5.15×10^{-4}	[22]
SERS	AgNPs	0.001-100	0.001	[23]
SERS	silica-coated nanoparticles	10^{-4} -100	10^{-4}	[24]
Fluorescence/SERS	GNPs@MIL-53(Al)	0.05-500 / 5×10^{-5} -1000	0.002 / 1.2×10^{-5}	This work

References

- 1 R. Gao, D. Li, Q. M. Zhang, S. Zheng, X. Ren, W. Deng, *Sens. Actuat. B-Chem.* 2021, **328**, 128960-128968.
- 2 P. C. Ray, *Angew. Chem.* 2006, **45**, 1151-1154.
- 3 W. N. Turner, C. I. Holdsworth, S. W. Donne, A. McCluskey, C. M. Bowyer, *New J. Chem.* 2010,

- 34**, 686-692.
- 4 Y. W. Zhou, Y. F. Wu, *Compos. Struct.* 2012, **94**, 580-592.
- 5 M. Fioravante, A. Shook, I. Thorpe, P. Rheingans, *Comp. Graph. Forum.* 2013, **32**, 311-320.
- 6 S. Munir, S. Hussain, S. Y. Park, *ACS Appl. Mater. Interfaces.* 2019, **11**, 37434-37441.
- 7 K. Pramanik, P. Sengupta, B. Majumder, P. Datta, P. Sarkar, *ACS Appl. Mater. Interfaces.* 2020, **12**, 36948-36956.
- 8 Y. Chen, Q. Zhong, Y. Wang, C. Yuan, X. Qin, Y. Xu, *RSC Adv.* 2019, **9**, 16566-16570.
- 9 X. Bi, X. Du, J. Jiang, X. Huang, *Anal. Chem.* 2015, **87**, 2016-2021.
- 10 Y. Kang, X. Xue, W. Wang, Y. Fan, W. Li, T. Ma, F. Zhao, Z. J. Zhang, *J. Phys. Chem. C.* 2020, **124**, 21054-21062.
- 11 J. L. Ma, B. C. Yin, X. Wu, B. C. Ye, *Anal. Chem.* 2017, **89**, 1323-1328.
- 12 Q. Lu, T. Huang, J. Zhou, Y. Zeng, C. Wu, M. Liu, H. Li, Y. Zhang, S. Yao, *Spectrochim Acta A.* 2021, **244**, 118893-118899.
- 13 A. P. Nagvenkar, A. Gedanken, *ACS Appl. Mater. Interfaces.* 2016, **8**, 22301-22308.
- 14 Y. Wang, J. Wang, T. Xie, L. Zhang, L. Yang, Q. Zhu, S. Liu, Y. Peng, X. Zhang, Q. Deng, *New J. Chem.* 2019, **43**, 7866-7873.
- 15 A. Yiğit, N. Alpar, Y. Yardım, M. C. elebi, Z. S,entürk, *Electroanalysis.* 2018, **30**, 1-11.
- 16 S. L. Reddy, C. Arul, Z. Liu, N. Lavanya, C. Sekar, *J. Electroanal Chem.* 2020, **878**, 114648-114659.
- 17 N. Sudhan, N. Lavanya, S. G. Leonardi, G. Neri, C. Sekar, *ACS Sensors* 2019, **19**, 3437-3451.
- 18 F. Nemati, M. Hosseini, R. Zare-Dorabei, F. Salehnia, M. R. Ganjali, *Sens. Actuat. B-Chem.* 2018, **273**, 25-34.
- 19 N. González, S. P. L. Corral, G. Zanini, H. Montejano, C. C. Acebal, *Analyst.* 2010, **145**, 2279-2285.
- 20 C. Du, C. Ma, J. Gu, L. Li, G. Chen, *ACS Sensors* 2020, **20**, 819-827.
- 21 R. Hu, R. Tang, J. Xu, F. Lu, *Anal. Chim. Acta.* 2018, **1034**, 176-183.
- 22 H. Zheng, D. Ni, Z. Yu, P. Liang, H. Chen, *Sens. Actuat B-Chem.* 2016, **231**, 423-430.
- 23 J. Hughes, E. L. Izake, W. B. Lott, G. A. Ayoko, M. Sillence, *Talanta* 2014, **130**, 20-25.
- 24 W. Luo, C. Zhu, S. Su, D. Li, Y. He, Q. Huang, C. Fan, *ACS Nano* 2010, **4**, 7451-7458.